

Analysis of the impact of storage conditions on the thermal recovery efficiency of low-temperature ATES systems

Bloemendal, Martin; Hartog, Niels

DOI

[10.1016/j.geothermics.2017.10.009](https://doi.org/10.1016/j.geothermics.2017.10.009)

Publication date

2018

Document Version

Accepted author manuscript

Published in

Geothermics

Citation (APA)

Bloemendal, M., & Hartog, N. (2018). Analysis of the impact of storage conditions on the thermal recovery efficiency of low-temperature ATES systems. *Geothermics*, 71, 306-319.
<https://doi.org/10.1016/j.geothermics.2017.10.009>

Important note

To cite this publication, please use the final published version (if applicable).
Please check the document version above.

Copyright

Other than for strictly personal use, it is not permitted to download, forward or distribute the text or part of it, without the consent of the author(s) and/or copyright holder(s), unless the work is under an open content license such as Creative Commons.

Takedown policy

Please contact us and provide details if you believe this document breaches copyrights.
We will remove access to the work immediately and investigate your claim.

Analysis of the impact of storage conditions on the thermal recovery efficiency of low-temperature ATEs systems

Martin Bloemendal^{1,2,*}, Niels Hartog^{2,3}

¹ Department of Water Management, Delft University of Technology, Delft, The Netherlands

² KWR, Watercycle Research Institute, Nieuwegein, The Netherlands

³ Faculty of Geosciences, Utrecht University, Utrecht, The Netherlands

*Corresponding author: Delft University of Technology, Department of Water Management, PO Box 5048, 2600 GA, Delft, The Netherlands, Email: j.m.bloemendal@tudelft.nl, Phone: +31625179849

Abstract

Aquifer thermal energy storage (ATES) is a technology with worldwide potential to provide sustainable space heating and cooling using groundwater stored at different temperatures. The thermal recovery efficiency is one of the main parameters that determines the overall energy savings of ATEs systems and is affected by storage specifics and site-specific hydrogeological conditions. Although beneficial for the optimization of ATEs design, thus far a systematic analysis of how different principal factors affect thermal recovery efficiency is lacking. Therefore, analytical approaches were developed, extended and tested numerically to evaluate how the loss of stored thermal energy by conduction, dispersion and displacement by ambient groundwater flow affect thermal recovery efficiency under different storage conditions. The practical framework provided in this study is valid for the wide range of practical conditions as derived from 331 low-temperature (<25°C) ATEs systems in practice.

Results show that thermal energy losses from the stored volume by conduction across the boundaries of the stored volume dominate those by dispersion for all practical storage conditions evaluated. In addition to conduction, the displacement of stored thermal volumes by ambient groundwater flow is also an important process controlling the thermal recovery efficiencies of ATEs systems. An analytical expression was derived to describe the thermal recovery efficiency as a function of the ratio of the thermal radius of the stored volume over ambient groundwater flow velocity (R_{th}/u). For the heat losses by conduction, simulation results showed that the thermal recovery efficiency decreases linearly with increasing surface area over volume ratios for the stored

28 volume (A/V), as was confirmed by the derivation of A/V -ratios for previous ATEs studies. In the presence of
 29 ambient groundwater flow, the simulations showed that for $R_{th}/u < 1$ year, displacement losses dominated
 30 conduction losses. Finally, for the optimization of overall thermal recovery efficiency as affected by these two
 31 main processes, the optimal design value for the ratio of well screen length over thermal radius (L/R_{th}) was
 32 shown to decrease with increasing ambient flow velocities while the sensitivity for this value increased. While in
 33 the absence of ambient flow a relatively broad optimum exists around an L/R_{th} -ratio of 0.5 to 3, at 40 m/year of
 34 ambient groundwater flow the optimal L/R_{th} -value ranges from 0.25 to 0.75). With the insights from this study,
 35 the consideration of storage volumes, the selection of suitable aquifer sections and well screen lengths can be
 36 supported in the optimization of ATEs systems world-wide.

37 **Nomenclature**

38	A	=	Surface area of the heat storage in the aquifer [m^2]
39	α	=	Dispersivity [m]
40	c_w	=	Volumetric heat capacity of water; 4.2×10^6 [$J/m^3/K$]
41	c_{aq}	=	Volumetric heat capacity of saturated porous medium; 2.8×10^6 [$J/m^3/K$]
42	D_{eff}	=	Effective dispersion [m^2/d]
43	D_T	=	Thermal dispersion [m^2/d]
44	$\Delta \bar{T}$	=	Average temperature difference between warm and cold well [$^{\circ}C$]
45	E	=	Energy [J]
46	η_{th}	=	Thermal efficiency [-]
47	i	=	Groundwater head gradient [-]
48	k	=	Hydraulic conductivity [m/d]
49	k_{Taq}	=	Thermal conductivity of water and particles; 2.55 [$W/m/K$]
50	L	=	Well screen length [m]
51	n	=	Porosity; 0.3 [-]
52	Q	=	Pumping rate of ATEs wells [m^3/d]
53	ρ	=	Water density; 1,000 [kg/m^3]
54	R	=	Thermal Retardation factor [-]
55	R_{th}	=	Thermal radius [m]
56	R_h	=	Hydraulic radius [m]

57	τ	=	Dimensionless time of travel parameter [-]
58	t_{sp}	=	Length of storage period [d]
59	T	=	Temperature [°K]
60	t	=	Time step [d]
61	u	=	Ambient groundwater flow velocity [m/d]
62	v	=	Flow velocity of the groundwater [m/d]
63	u_*	=	Velocity of the thermal front [m/d]
64	V	=	Yearly (permitted or actual) storage volume groundwater [m ³]

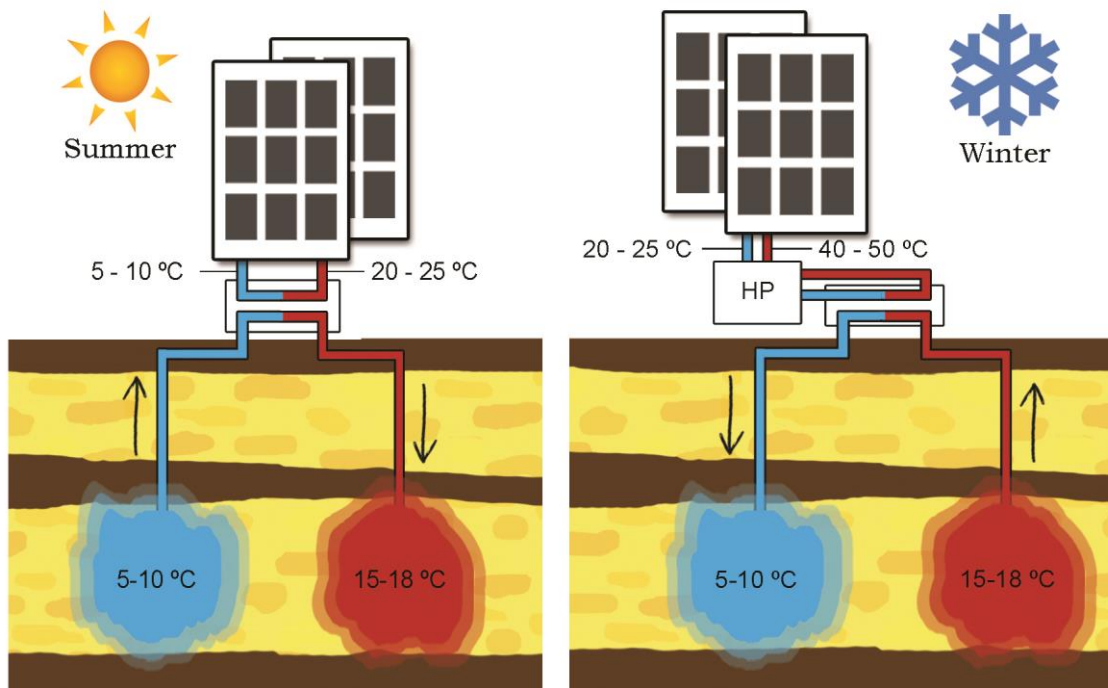
65 **1. Introduction**

66 World-wide efforts aim to reduce greenhouse gas emissions and to meet energy demands sustainably (EU, 2010;
67 SER, 2013; UN, 2015). Global demand for heating and cooling in the built environment accounts for about 40%
68 of the total energy consumption (EIA, 2009; Kim et al., 2010; RHC, 2013). In reducing this demand, the use of
69 Aquifer Thermal Energy Storage¹ (ATES) systems for space heating and cooling has a high potential in the
70 many regions worldwide that have substantial seasonal, or sometimes diurnal, variations in ambient air
71 temperature combined with favorable geohydrological conditions (Bloemendal et al., 2015).

72 Although much of the early ATES research has focused on storage at high temperatures (Molz et al., 1983; Molz
73 et al., 1978; Nagano et al., 2002; Réveillère et al., 2013; Tsang, 1978), most practical experience with seasonal
74 ATES systems has in recent years been gained in particularly several European countries (Eugster and Sanner,
75 2007; Fry, 2009; Haehnlein et al., 2010; Willemsen, 2016). These ATES systems seasonally store thermal
76 energy at relatively low temperatures (<25°C) alternating between cooling and, assisted by a heat pump, heating
77 mode (Figure 1). The number of ATES systems has grown rapidly in the past decade particularly in The
78 Netherlands (Figure 2), a country with a moderate climate and widespread presence of thick sedimentary
79 aquifers. The introduction of progressively stricter energy efficiency requirements for buildings (Energy
80 Performance Coefficient (EPC), stimulated the adoption of ATES in the built environment. As a result, there are
81 currently almost 2,000 systems in operation in relatively shallow sandy aquifers (typically 20-150 m.b.g.l.).

¹ Also often referred to as open loop geothermal storage systems. Closed loop or borehole heat exchangers also have a high potential for energy savings. In this paper the focus is on ATES systems because they provides a more (cost) effective option for large scale cooling and heating in urban areas mainly for utility buildings and large scale housing complexes

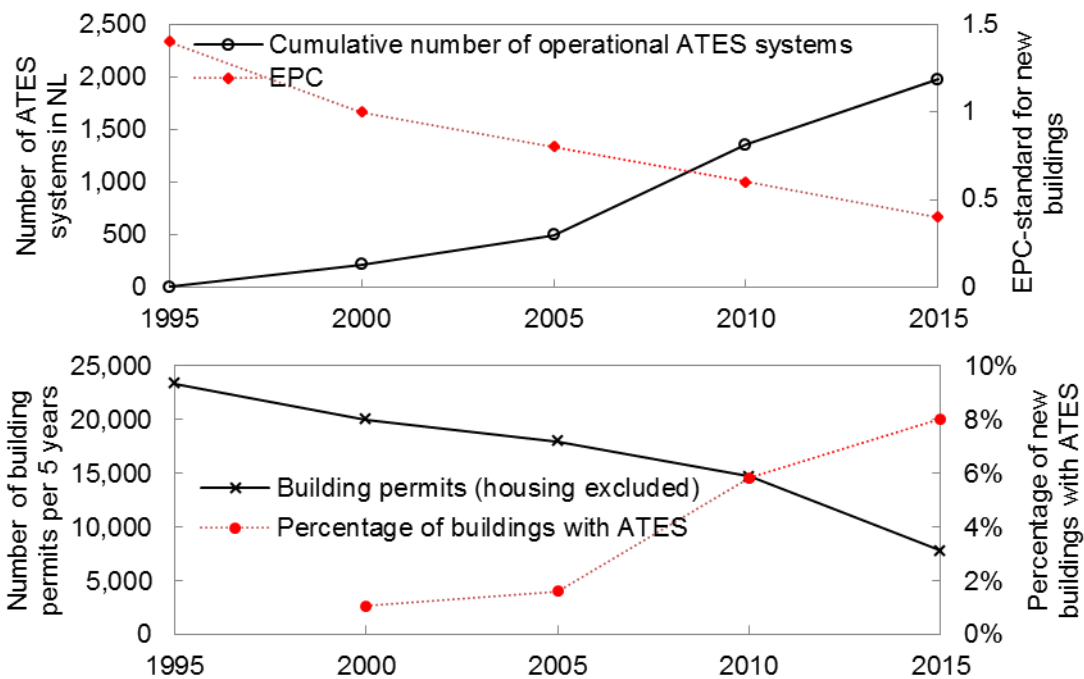
82 For both an optimal energy performance of an ATES system as well as minimal effect on the subsurface, the
83 thermal energy recovery efficiency needs to be as high as possible. Under these conditions, the electricity
84 required for groundwater pumping and heat pump (Figure 1) is minimized.



85
86 *Figure 1, Illustration of the basic working principle of a low-temperature seasonal ATES system. Left: in direct cooling mode while storing*
87 *heat for winter. Right: vice-versa in heating mode supported by a heat pump while storing cooling capacity for summer*

88 Previous studies have shown that the thermal recovery efficiency of ATES systems are negatively affected by
89 thermal energy losses from the stored volume by conduction, diffusion and dispersion (Doughty et al., 1982;
90 Sommer et al., 2014). While for high temperature ($>45^{\circ}\text{C}$) ATES systems, the negative impact of the buoyancy
91 of the stored hot water on thermal recovery efficiency typically needs to be considered (Lopik et al., 2016;
92 Zeghici et al., 2015), this can be neglected for low temperature ATES systems (Doughty et al., 1982; Zuurbier et
93 al., 2013). However, as these low temperature ATES systems are typically targeting relatively shallow aquifers,
94 the impact of stored volume displacement by ambient groundwater flow requires consideration. Although the
95 impact of ambient groundwater flow on injected and recovered water volumes has been studied (Bear and
96 Jacobs, 1965; Ceric and Haitjema, 2005), the impact of ambient groundwater flow on thermal recovery
97 efficiency in ATES systems, has thus far not been explored. Moreover, it is unclear how the combined impact of
98 these processes (dispersion, conduction and advection) affects the thermal recovery efficiency of ATES systems
99 under practical conditions and how the efficiency can be optimized.

100 Therefore, the aim of this study is to use analytical methods to elucidate the impact of ambient groundwater flow
 101 and conduction and dispersion on the thermal recovery efficiency of ATEs systems and to use numerical
 102 methods to assess how the combined heat loss by multiple processes can be minimized. As a practical
 103 framework for the conditions investigated, the wide range of ATEs system characteristics and hydrogeological
 104 conditions in the Netherlands was used. The resulting insights are meant to provide a useful basis to enable the
 105 optimization of the thermal recovery efficiency of ATEs systems and to further optimize development for
 106 sustainable heating and cooling of buildings world-wide.



107

108 *Figure 2, Top: increase of number of ATEs systems during recent years in the Netherlands along with the decreasing EPC-standard for*
 109 *dwellings. The EPC value is a normalized value of the expected energy use of a building (CBS, 2016a; LGR, 2012; Ministry-of-Internal-*
 110 *affairs, 2012). Bottom: The increasing percentage of new buildings build with ATEs system (CBS, 2016a, b)*

111 2. Materials and Methods

112 2.1 Theory of heat transport and recovery during ATEs

113 *Definition of thermal recovery efficiency for ATEs systems*

114 The thermal energy stored in an ATEs system can have a positive and negative temperature difference between
 115 the infiltrated water and the surrounding ambient groundwater, for either heating or cooling purposes (Figure 1).
 116 In this study the thermal energy stored is referred to as heat or thermal energy; however, all the results discussed
 117 equally apply to storage of cold water used for cooling. As in other ATEs studies (Doughty et al., 1982;

118 Sommer, 2015), the recovery efficiency (η_{th}) of an ATES well is defined as the amount of injected thermal
 119 energy that is recovered after the injected volume has been extracted. For this ratio between extracted and
 120 infiltrated thermal energy (E_{out}/E_{in}), the total infiltrated and extracted thermal energy is calculated as the
 121 cumulated product of the infiltrated and extracted volume with the difference of infiltration and extraction
 122 temperatures ($\Delta T = T_{in} - T_{out}$) for a given time horizon (which is usually one or multiple storage cycles), as
 123 described by:

$$124 \quad \eta_{th} = \frac{E_{out}}{E_{in}} = \frac{\int \Delta T Q_{out} dt}{\int \Delta T Q_{in} dt} = \frac{\Delta \bar{T}_{out} V_{out}}{\Delta \bar{T}_{in} V_{in}} \quad (1),$$

125 with, Q being the well discharge during time step t and $\Delta \bar{T}$ the weighted average temperature difference
 126 between extraction and injection. Injected thermal energy that is lost beyond the volume to be extracted is
 127 considered lost as it will not be recovered. To allow unambiguous comparison of the results the simulations in
 128 this study are carried out with constant yearly storage and extraction volumes ($V_{in} = V_{out}$).

129 *Loss of heat due to displacement by ambient groundwater flow*

130 Significant ambient groundwater flow is known to occur at ATES sites (Bonte et al., 2013b; Groot, 2013; Hartog
 131 et al., 2013), which leads to displacement of the injected volumes (Bear and Jacobs, 1965; Bonte et al., 2013a).
 132 This may lead to significant reduction in the thermal energy recovery efficiency of ATES systems as ambient
 133 groundwater flow (u) contributes to thermal losses by displacing the injected water during storage. The heat
 134 transport velocity (u_*) is retarded with respect to ambient groundwater flow (Doughty et al., 1982; Hecht-
 135 Mendez et al., 2010) due to heat storage in the aquifer solids. The thermal retardation (R) depends on porosity
 136 (n) and the ratio between volumetric heat capacities of water (c_w) and aquifer (c_{aq} , with $c_{aq} = nc_w + (1-n)c_s$ and c_s
 137 the solids volumetric heat capacity), following:

$$138 \quad u_* = \frac{1}{R} u = \frac{nc_w}{c_{aq}} u \approx 0.5 \cdot u \quad (2).$$

139 Resulting in a heat transport velocity at approximately 50% of the groundwater flow velocity (u). Under
 140 conditions of ambient groundwater flow, thermal energy stored in an aquifer will thus be displaced and can only
 141 be partly (Bear and Jacobs, 1965) recovered.

142 *Loss of heat by dispersion and conduction*

143 Mechanical dispersion and heat conduction spread the heat over the boundary of the cold and warm water bodies
144 around the ATES wells. As a consequence of the seasonal operation schedule, diffusion losses are negligible
145 (Anderson, 2005; Bear, 1979). Both other processes are described by the effective thermal dispersion (D_{eff})
146 which illustrates the relative contribution of both processes to the losses, following:

147
$$D_{eff} = \frac{\kappa_{Taq}}{nc_w} + \alpha \frac{v}{n} \quad (3),$$

148 where, the first term represents the conduction, which depends on the volumetric heat capacity (c_w) of water and
149 the thermal conductivity (κ_{Taq}) and porosity (n) of the aquifer material which are considered to remain constant at
150 about 0.15 [m²/d] in a sandy aquifer with porosity of 0.3. The rate at which conduction occurs can be determined
151 by the increasing standard deviation: $\sigma = \sqrt{2D_T t}$, with D_T , the effective thermal dispersion (the left hand term
152 of Equation (3) and t the storage time. For half a year storage period the rate at which heat moves through
153 conduction is about 7m.

154 The second term of Equation (3) represents the mechanical dispersion, which depends on the dispersivity (α) of
155 the subsurface, porosity and the flow velocity of the water (v), which is the sum of the force convection due to
156 the infiltration and extraction of the well, as well as the ambient groundwater flow (u). For ATES wells that fully
157 penetrate an aquifer confined by aquitards, the dispersion to cap and bottom of the thermal cylinder (Figure 3) is
158 negligible due to the lack of flow (Caljé, 2010; Doughty et al., 1982). With regularly applied values of 0.5 to 5
159 for the dispersivity (Gelhar et al., 1992), the dispersion is in the same order of magnitude as the conduction at
160 flow velocities of 0.01 to 0.1 m/d.

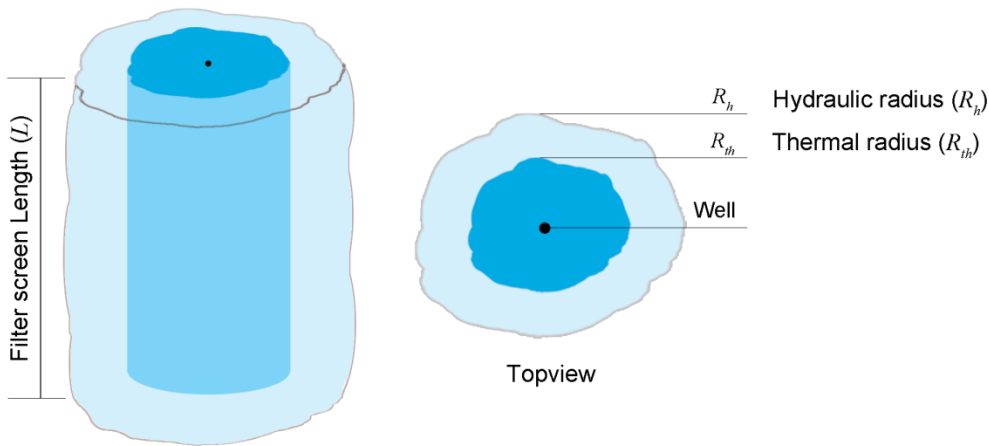
161 Since losses due to mechanical dispersion and conduction occur at the boundary of the stored body of thermal
162 energy, the thermal recovery efficiency therefore depends on the geometric shape of the thermal volume in the
163 aquifer (Doughty et al., 1982). Following Doughty (1982), the infiltrated volume is simplified as a cylinder with
164 a hydraulic radius (R_h) defined as:

165
$$R_h = \sqrt{\frac{V_{in}}{n\pi L}} \quad (4)$$

166 and for which the thermal radius (R_{th}) is defined as:

167
$$R_{th} = \sqrt{\frac{c_w V_{in}}{c_{aq} \pi L}} = \sqrt{\frac{n c_w}{c_{aq}}} R_h = \sqrt{\frac{1}{R}} R_h \approx 0.66 \cdot R_h \quad (5).$$

168 The size of the thermal cylinder thus depends on the storage volume (V), screen length (L , for a fully screened
 169 aquifer), porosity (n) and water and aquifer heat capacity (Figure 3). This equation is approximate because
 170 heterogeneities and partially penetration of the screens are ignored. Doughty et al. (1982) introduced a
 171 dimensionless ratio of screen length and the thermal radius (L/R_{th}) as a parameter to describe thermal recovery
 172 efficiency of ATES systems for a particular stored thermal volume. They found that the ATES recovery
 173 efficiency has a flat optimum between a value of 1 and 4 for this ratio.



174

175 *Figure 3, Simplified presentation of the resulting subsurface thermal and hydrological storage cylinder for an ATES system for homogeneous*
 176 *aquifer conditions.*

177 Losses due to interaction between ATES systems are not taken into account in this research. Also interaction
 178 between the warm and cold well of the same system is not taken into account as this is prevented by the
 179 permitting requirement to ensure sufficient separation distance (three times the thermal radius).

180 **2.2 Numerical modeling of ATES**

181 As losses due to conduction, dispersion and displacement occur simultaneously, MODFLOW (Harbaugh et al.,
 182 2000) simulations is used to evaluate their combined effect on recovery efficiency. For the simulation of ambient
 183 groundwater flow and heat transport under various ATES conditions, a geohydrological MODFLOW model
 184 (Harbaugh et al., 2000) coupled to the transport code MT3DMS (Hecht-Mendez et al., 2010; Zheng and Wang,
 185 1999). These model codes use finite differences methods to solve the groundwater and (heat) transport equations
 186 . This allows for simulation of infiltration and extraction of groundwater in and from groundwater wells and

187 groundwater temperature distribution, as was done in previous ATEs studies e.g. (Bonte, 2013; Caljé, 2010;
188 Sommer, 2015; Visser et al., 2015). In the different modeling scenarios the storage volume is varied between
189 12,000 and 300,000 m³ with flow rates proportionally ranging from 8 to 200 m³/hour, screen lengths between 10-
190 105 m and ambient groundwater flow velocities between 0 and 50 m/y following the characteristics from Dutch
191 practice as will be introduced in the next section. Density differences are neglected as this is considered a valid
192 assumption (Caljé, 2010) for the considered ATEs systems that operate within a limited temperature range
193 (<25°C). The parameter values of the model are given in Table 1, the following discretization was used:

- 194 - Model layers; the storage aquifer is confined by two 10 m thick clay layers. The storage aquifer is
195 divided in 3 layers, a 5 m thick upper and lower layer, the middle layers' thickness is changed according
196 to the required screen length of the modeled scenario.
- 197 - The spatial discretization used in horizontal direction is 5 x 5 m at well location, gradually increasing to
198 100 x 100 m at the borders of the model. A sufficiently large model domain size of 6x6km was used to
199 prevent boundary conditions affecting (<1%) simulation results. The gradually increasing cell size with
200 distance from the wells results the cell size of 15m at 200m of the well. This discretization is well
201 within the minimum level of detail to model the temperature field around ATEs wells as was identified
202 by Sommer (2014).
- 203 - A temporal discretization of one week is used, which is sufficiently small to take account for the
204 seasonal operation pattern and resulting in a courant number smaller than 0.5 within the area around the
205 wells where the process we care about occur. The simulation has a horizon of 10 years, sufficiently long
206 to achieve stabilized yearly recovery efficiencies.

207 The PCG2 package is used for solving the groundwater flow, and the MOC for the advection package simulating
208 the heat with a courant number of 1. To set the desired ambient groundwater flow velocity for the different
209 scenarios simulated, the constant hydraulic head boundaries were used to set the required hydraulic gradient. In
210 the aquifer an ATEs doublet is placed with a well distance of five times the maximum thermal radius of the
211 wells to avoid mutual interaction between the warm and cold storage volumes. In scenarios with groundwater
212 flow, the ATEs wells are oriented perpendicular to the flow direction.

213 The energy demand profile of ATEs systems varies due to variations in weather conditions and building use
214 which is of importance for the actual value of the thermal efficiency. For 12 varying scenarios the efficiencies
215 are determined for both a weather dependent and the regular energy demand profile, showing that the

216 efficiencies of the corresponding conditions differ. However, they show the same relation according to the
 217 changes in conditions; the Pearson correlation coefficient of the two simulation result collections is 0.97. Based
 218 on this evaluation all simulations are done with one basic energy demand profile, to allow for comparison with
 219 the analytical solutions also the constant storage volume energy demand pattern will be used; heat injection,
 220 storage, extraction and again storage during 13 weeks each as is commonly done in other ATEs research
 221 (e.g.(Sommer et al., 2014; Zuurbier et al., 2013)).

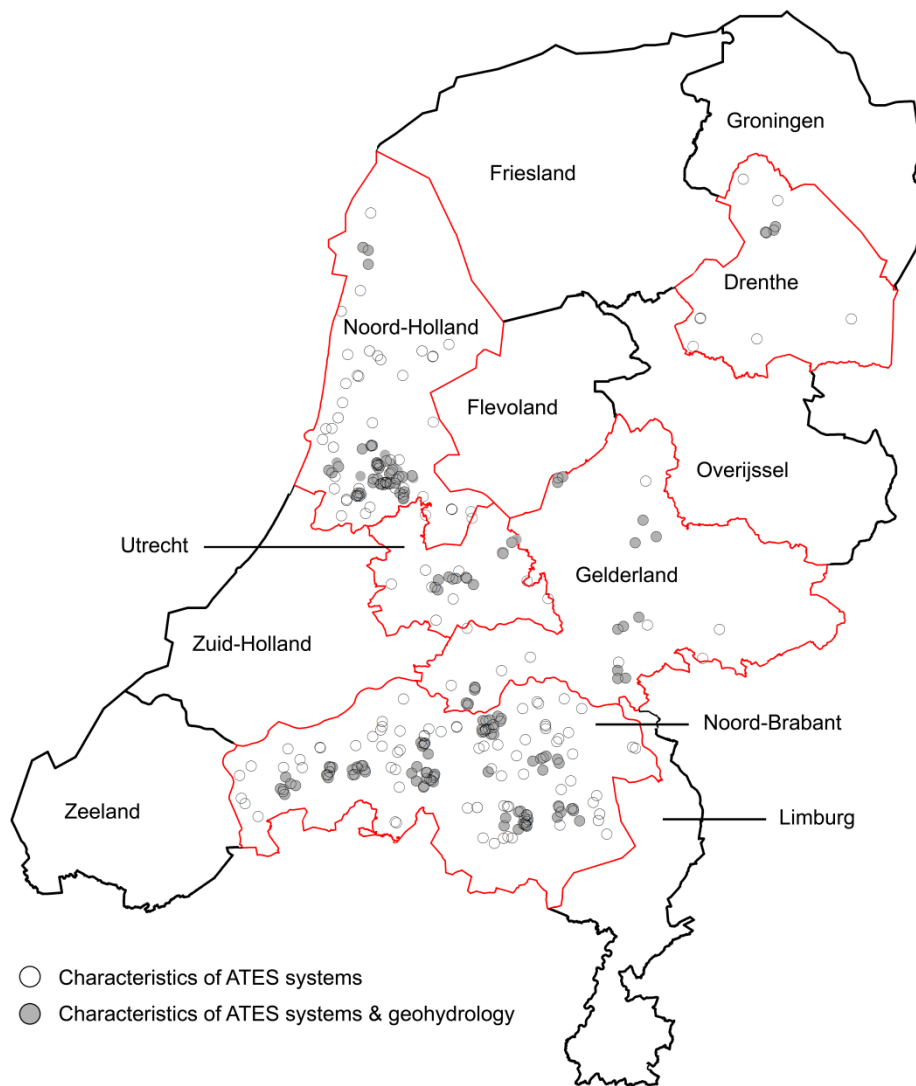
222 *Table 1, MODFLOW simulation parameter values (Caljé, 2010; Hecht-Mendez et al., 2010)*

Parameter	value
Horizontal conductivity aquifers	25 m/d
Horizontal conductivity aquitards	0.05 m/d
Longitudinal dispersion	1 m
Transversal dispersion	0,1 m
Bulk density	1890 kg/m ³
Bulk thermal diffusivity	0.16 m ² /day
Solid heat capacity	880 J/kg °C
Thermal conductivity of aquifer	2.55 W/m °C
Effective molecular diffusion	1·10 ⁻¹⁰ m ² /day
Thermal distribution coefficient	2·10 ⁻⁴ m ³ /kg

223 **2.3 Characteristics and conditions of ATEs systems in The Netherlands**

224 *Characteristics of the ATEs systems*

225 Data on the location, permitted yearly storage volume, pump capacity and screen length of 331 ATEs systems in
 226 The Netherlands (15 % of total number of systems) were obtained from provincial databases that keep combined
 227 records for ATEs characteristics of interest for this research (Provinces of Gelderland, Noord-Brabant, Noord-
 228 Holland, Utrecht and Drenthe, Figure 4).



229

230 *Figure 4. Locations of selected ATES systems from 5 provincial databases. Other provinces have ATES systems as well but in their databases*
 231 *some characteristics required for this evaluation were missing, Open circles indicate locations for which ATES characteristics were*
 232 *available. Filled circles indicate locations for which also the local geohydrological conditions were available.*

233 *Geohydrological conditions at ATES systems*

234 For a geographically representative subset of 204 ATES systems (Figure 4) it was possible to extract available
 235 aquifer thickness and derive estimates on the ambient groundwater flow, as this additional data are not available
 236 in the provincial databases. These estimates are based on hydraulic conductivity and head gradients derived from
 237 the Dutch geologic databases (TNO, 2002a) for the coordinates of these ATES systems. The groundwater head
 238 gradient is read from equipotential maps (TNO, 2002a) while the hydraulic conductivity and aquifer thickness is
 239 obtained from local soil profiles in the REGIS II (TNO, 2002a, b) subsurface model of the Netherlands and
 240 literature values for hydraulic conductivity (Bear, 1979; Kasenow, 2002) corresponding to the soil profiles from
 241 the bore logs. The data are abstracted and processed for the aquifer regionally targeted for ATES systems,

242 therefore, ATEs systems with wells installed in other aquifers are excluded from the local analysis. Legal
 243 boundaries are also taken into account, in Noord-Brabant for instance it is not allowed to install ATEs systems
 244 deeper than 80 m below surface level, so any aquifer available below 80 m is disregarded for the systems in this
 245 province. For all locations a porosity value of 30% is assumed, a value common for Dutch sandy aquifers
 246 (Bloemendal et al., 2015; NVOE, 2006; SIKB, 2015a).

247 3. Results

248 3.1 ATEs system properties in The Netherlands

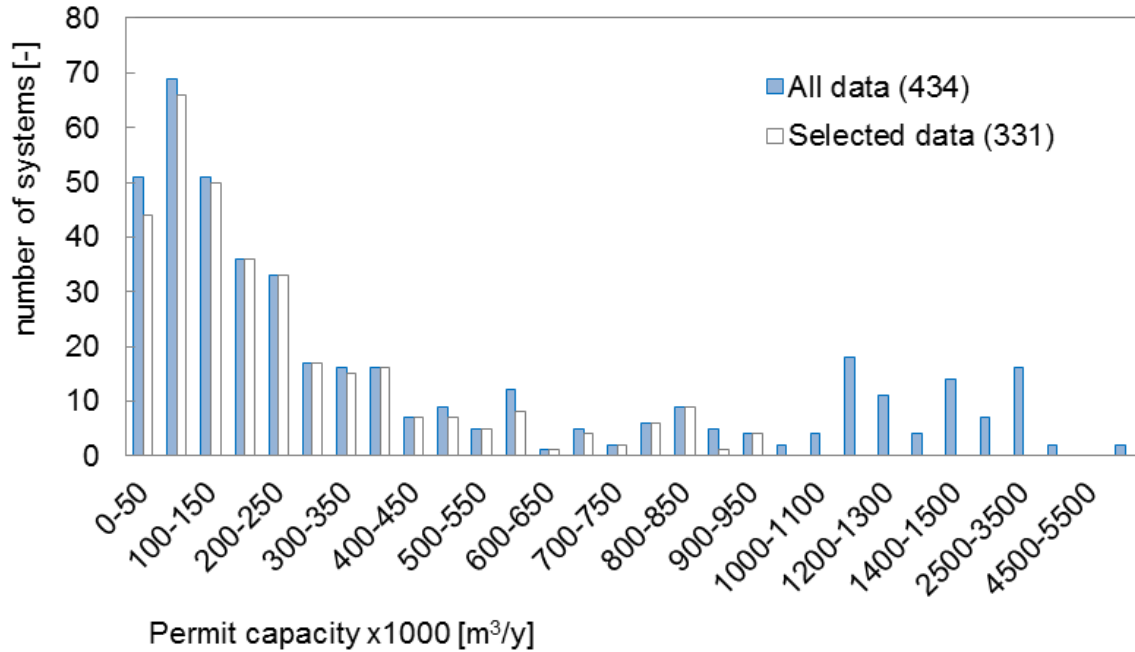
249 *Permitted capacity and screen length*

250 The permitted capacity of the ATEs systems ranges up to 5,000,000 m³/year but most (~70%) are smaller than
 251 500,000 m³/year (Figure 5, Table 2). The observed differences in ATEs system characteristics for the different
 252 provinces were limited and therefore not presented separately.

253 *Table 2, ATEs system characteristics in provincial datasets selected for this study*

	Number of ATEs systems	Permitted capacity (V) [m ³ /y]			Installed screen length (L) [m]		
		0.25 perc.	Average	0.75 perc.	0.25 perc.	Average	0.75 perc.
Initial data	434	90,000	539,000	674,000	20	37	45
selected data	331	80,000	244,000	320,000	20	32	40

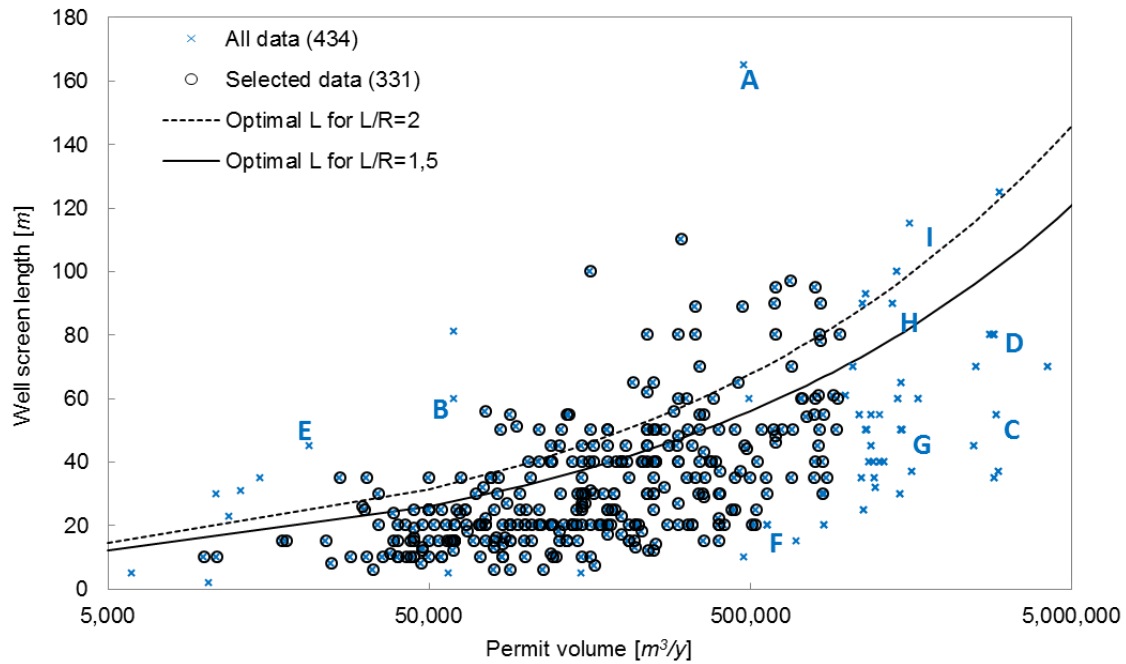
254



255

256 *Figure 5, Frequency distribution of dataset according to permitted yearly storage volume of groundwater. Distribution of well design*
 257 *metrics of selected data is shown separately.*

258 To be able to evaluate the resulting geometry of the storage volume in evaluating dispersion and conduction
 259 losses it is assumed that the thermal energy is stored in a single cylindrical volume. Most ATEs systems in the
 260 Netherlands are single doublet systems or multiple doublet systems with clustered warm and cold wells.
 261 However, particularly for some larger systems, warm and cold wells are not clustered, due to for example spatial
 262 planning or geohydrological and/or geotechnical reasons (Bloemendal et al., 2015). Unfortunately the provincial
 263 data did not include the number or type of well pairs. Therefore the data was filtered for the systems for which a
 264 multiple number of well pairs or other deviating aspects could be confirmed. Those systems mostly belong to the
 265 largest 10 % of the systems, or belong to outliers in the data distribution of screen length over stored volume,
 266 and were therefore excluded.. For the largest systems, multiple doublets were confirmed for several systems (e.g.
 267 C, D, F,G, H, I). In addition, some errors were found in the data of the provincial databases, inconsistent,
 268 incomplete entries (e.g. E) with errors (e.g. impossible short or long screen lengths), such as monowell systems
 269 with only one very long screen which should be divided in two screens (A and B in Figure 6). As a result of this
 270 validation of the dataset, 331 systems were selected for further evaluation (Figure 6). The data used for analysis
 271 represents about 15 % of the approximately 2,000 systems operational in the Netherlands (Willemsen, 2016).



272

273 Figure 6, Dataset characteristics; outliers are excluded from the dataset. A, B=monowells with only top of upper and bottom of lower filter
 274 in the data, C=University Campus ~6 doublets, D=Office with 3 doublets, E=Office building with only extracted volume of one year
 275 available in data, unrealistically small for size of building, F=office with 4 doublets, G=Hospital with 4 doublets, H=conference center with
 276 2 monowells, I=Office with 3 doublets

277 *Geohydrological conditions*

278 Table 3 shows the overall geohydrological characteristics at the location of 204 ATES systems. Both hydraulic
 279 conductivity and ambient groundwater flow velocity show a wide range.

280 Table 3, Ranges in geohydrological characteristics of the 204 ATES systems under consideration, for which geohydrological conditions
 281 could be retrieved.

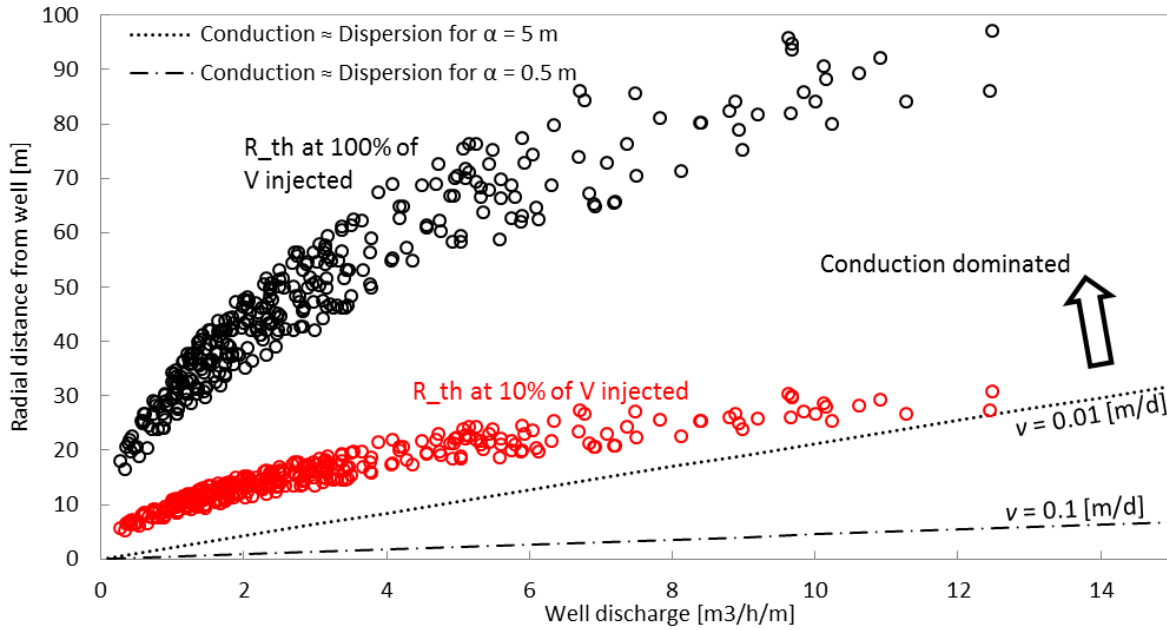
Available aquifer thickness range	Hydraulic conductivity Range	Groundwater flow range
[m]	[m/d]	[m/y]
30-180	5-45	3-100

282 **3.2 Analytical evaluation of ATES thermal recovery**

283 *Loss of thermal energy due to dispersion and conduction*

284 Both conduction and dispersion losses occur at the boundary of the stored thermal cylinder. Following Equation
 285 (3); near the well, where flow velocity of the infiltrated water (v) is high, dispersion dominates the conduction
 286 term, while further from the well, the effects of dispersion decreases. Equation (3) and the values for the
 287 dispersion and aquifer properties in Table 1 are now used to identify the distance from the well at which the
 288 dominating process contributing to loss, changes from dispersion to conduction, Figure 7. The pump capacity
 289 data of the ATES systems together with the storage volume and screen length are used to plot the thermal radii

290 of the systems with respect to their maximum specific discharge, showing that even assuming a relatively high
 291 dispersivity of 5 m, beyond 10% of permitted storage volume infiltration, conduction is dominating in the
 292 dispersivity equation, indicating that at full storage capacity conduction losses will be dominating.



293

294 *Figure 7. Lines: the relation between specific well discharge and radial distance at which the radial flow velocities where conduction and*
 295 *dispersion are equal (Eq. 3) for the outer-bounds of the range of thermal dispersivity regularly applied in literature. Open circles the*
 296 *thermal front of the ATES systems in the data at different storage capacities related to their specific well discharge .*

297 When the infiltration continues, the movement of the thermal front is dominated by the advective heat transport

298 of the injection. , The (high) dispersion losses that occur at the high flow velocities close to the well are

299 ”overtaken” when infiltration of heat continues, resulting in sharp heat interface as the infiltration volume

300 increases. This sharp interface remains sharp during infiltration because the heat injected by the well travels

301 faster than the standard deviation for the conduction ($\sigma = \sqrt{2D_r t}$). During storage and extraction the interface

302 will become less sharp due to respectively conduction and the opposite effect of these mechanisms. The heat that

303 thus stays behind causes that efficiency improves and stabilizes over multiple storage cycles. From which it is

304 concluded that losses can be minimized by minimizing the total surface area of the circumference and the cap

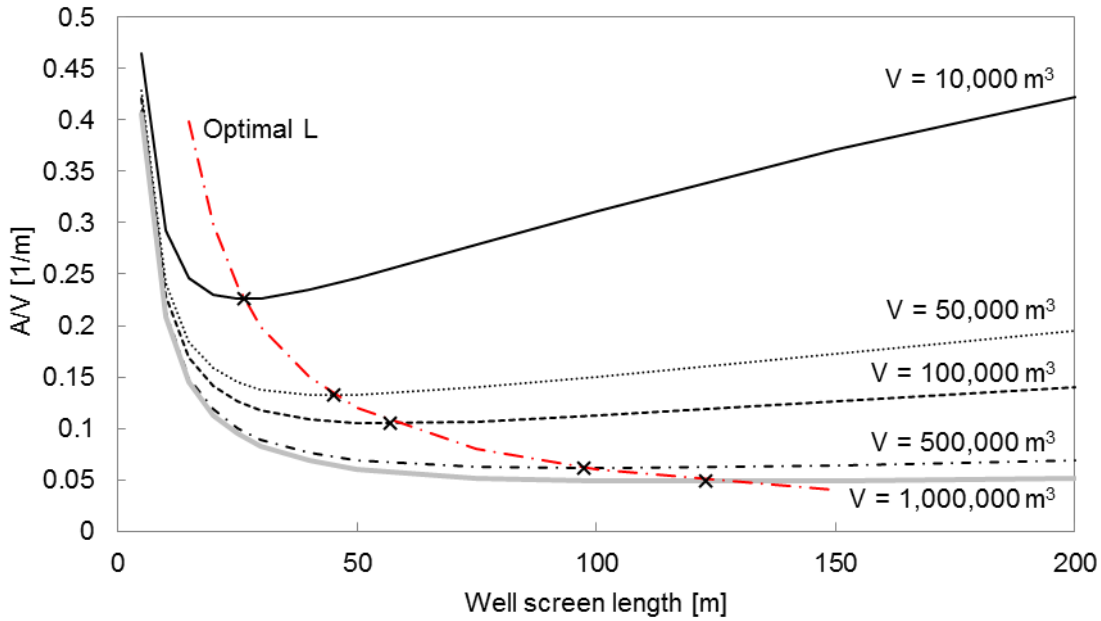
305 and bottom of the thermal cylinder (A) of the stored heat volume (V) in the aquifer. This can be done by

306 identifying an appropriate screen according to the required storage volume and local conditions, in order to

307 minimize the surface area – volume ratio;

308
$$\frac{A}{V} = \frac{2\pi R_{th}^2 + 2\pi R_{th} L}{\pi R_{th}^2 L} = \frac{2}{L} + \frac{2}{R_{th}} \quad (6).$$

309 For any given storage volume an optimal screen length exists at which conduction and dispersion losses are
 310 minimal at the screen length - thermal radius ratio (L/R_{th}) is 2, when the diameter of the cylindrical storage
 311 volume is equal to its screen length. From Figure 8 can be seen that for larger storage volumes the A/V -ratio is
 312 smaller, and less sensitive at larger screen lengths, exhibiting a relatively flat minimum compared to small
 313 storage volumes. Although the absolute losses increase with increasing storage volume, the relative losses are
 314 smaller.



315

316 *Figure 8, The A/V values for different storage volumes and well screen lengths*

317 To identify the optimal screen length the derivative for surface area of the thermal cylinder is equated to zero,
 318 which results in an expression for optimal screen length as a function of required storage volume;

$$319 \quad A = 2 \frac{c_w V}{c_a L} + 2\pi \sqrt{\frac{c_w V}{\pi c_a L}} L \rightarrow A' = \frac{-2\pi c_w V}{c_a L^2} + \pi \sqrt{\frac{c_w V}{\pi c_a}} \frac{1}{\sqrt{L}} \rightarrow L \approx 1.23 \cdot \sqrt[3]{V} \quad (7).$$

320 Consequently, relatively small storage volumes experience higher losses due to dispersion losses. Because there
 321 is no or little flow to and from the confining layers of an ATEs well, conduction losses along the interface with
 322 the confining soil layers may differ from the ones around the circumference. Therefore Doughty et al. (1982)
 323 distinguished between the two in their research to optimize well design, to account for the reduced conduction
 324 losses to confining layers after several storage cycles. Their Simulation showed that efficiency increases with the
 325 first number of storage cycles and found that the optimal ratio between screen length and thermal radius (L/R_{th})
 326 has a flat optimum around 1.5 when taking into account different thermodynamic properties of aquifers and

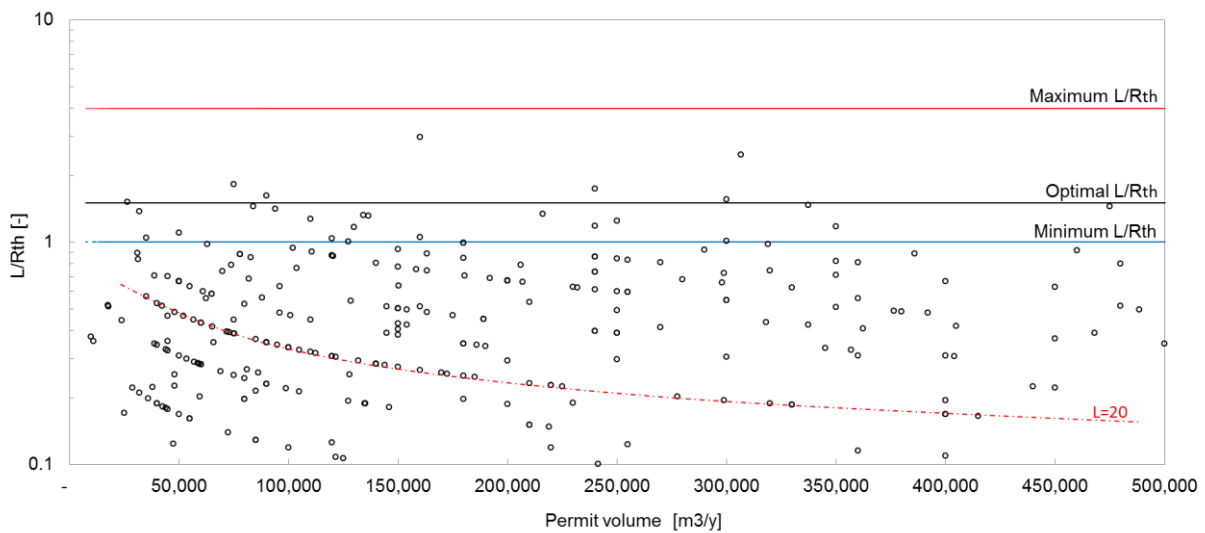
327 aquitards. Substituting the expression for the thermal radius (R_{th} , Equation (5)) in the optimal relation of
 328 $L/R_{th}=1.5$ gives the optimal screen length (L) as a function of storage volume (V);

329
$$L = \sqrt[3]{\frac{2.25 c_w V}{c_a \pi}} \approx 1.02 \cdot \sqrt[3]{V} \quad (8).$$

330 This shows that the solution for the screen length results in the same third root of the storage volume, only with a
 331 smaller constant 1.02 [-] instead of 1.23 [-] as was derived from the optimal A/V-ratio solution, Equation (6).

332 This is the case because over multiple cycles, the conduction losses to “cap & bottom” decrease; losses from
 333 earlier cycles dampen the losses during following cycles.

334 From the lines for L/R_{th} is 1.5 it can be seen that on average, screen lengths are designed far from optimal with
 335 respect to minimizing conduction losses. Doughty et al. (1982) however, found a flat optimum for L/R_{th} -value,
 336 thus it may also be acceptable when the L/R_{th} -value is between 1 and 4, based on the moment of deflection of the
 337 L/R_{th} -curve constructed by Doughty et al (1982). However most systems have L/R_{th} -values lower than 1,
 338 indicating that screen lengths used in Dutch practice are relatively short (Figure 9). Analysis shows that 56% of
 339 the ATEs systems with an $L/R_{th}<1$ have insufficient aquifer thickness available for longer screens.



340
 341 *Figure 9, L/R_{th} -value relative to permit volume of ATEs systems in practice, combined with minimum ($L/R_{th} = 1$), maximum ($L/R_{th} = 4$) and*
 342 *optimal ($L/R_{th} = 1.5$) L/R_{th} for conduction and dispersion losses*

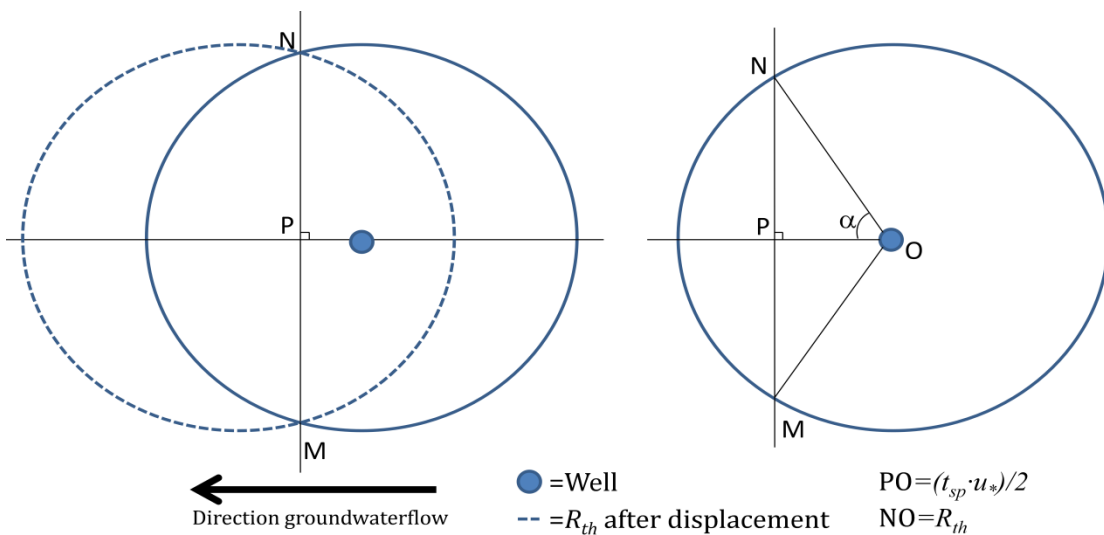
343 *The effect of ambient groundwater flow on recovery efficiency*

344 For the analysis of the impact of ambient groundwater flow on the recovery efficiency, it is assumed that a
 345 cylindrical shape of the injected volume is maintained during displacement. Ceric and Haitjema (2005)

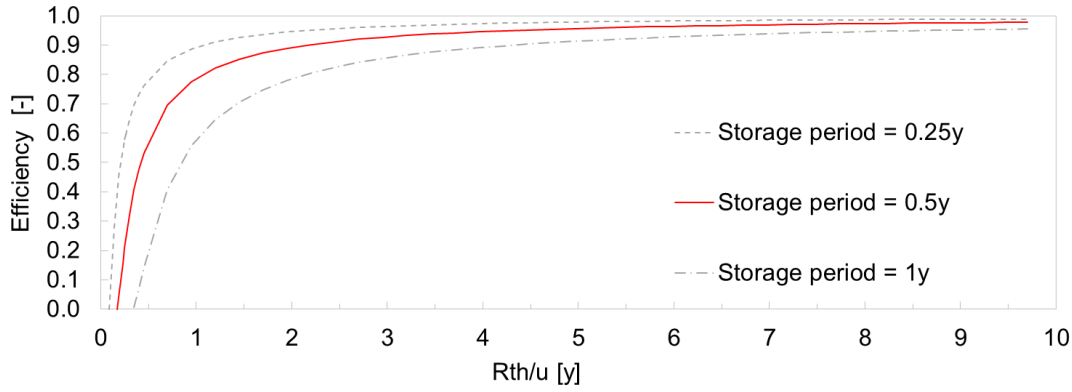
346 determined that this assumption is valid for conditions where their dimensionless time of travel parameter τ ,
 347 (Ceric and Haitjema, 2005) is smaller than one;

348
$$\tau = \frac{2\pi(ki)^2 L t_{sp}}{nQ} = \frac{2\pi n u^2 L t_{sp}}{Q} \quad (9).$$

349 The groundwater head gradient (i), hydraulic conductivity (k), screen length (L) and pumping rate (Q) of the
 350 ATES systems in the data are used to determine the time of travel parameter for each system. The only unknown
 351 is the length of storage period (t_{sp}). With an average storage period of 183 days (half a year) only one of
 352 calculated τ values for the 204 ATES systems was larger than one; a very small system in high ambient
 353 groundwater flow velocity. On top of meeting the requirement of Ceric and Haitjema, the thermal retardation
 354 also causes the heat to flow at half the speed of water, which then makes the assumption of preservation of a
 355 cylindrical shape during displacement an acceptable simplification. These conditions allow the definition of the
 356 recovery efficiency as a function of the overlapping part of the cylinders, with and without the displacement
 357 induced by ambient groundwater flow. Assuming that the ambient groundwater flow is horizontal, the surface
 358 area of the thermal footprints before and after displacement with the groundwater flow represents this efficiency,
 359 Figure 10 (top).



360



361

362 *Figure 10, Top: schematic overview of calculating the overlapping surface area of 2 identical thermal cylinders. Bottom: the derived*
 363 *analytical relation between losses and the thermal radius - groundwater flow velocity ratio.*

364 Goniometric rules are used to express the overlapping surface area ($A_{overlap}$) of the thermal footprint as a function
 365 of groundwater flow velocity and thermal radius, as follows:

$$366 \quad A_{overlap} = 2R_{th}^2 a \cos\left(\frac{t_{sp}u_*}{2R_{th}}\right) - t_{sp}u_* \sqrt{R_{th}^2 - \frac{1}{4}(t_{sp}u_*)^2} \quad (10)$$

367 in which the velocity of the thermal front ($t_{sp}u_*$) is 2 times PO in Figure 10 (top). Substituting the relation
 368 between efficiency (η_{th}), thermal footprint ($A_{footprint}$) and overlapping area:

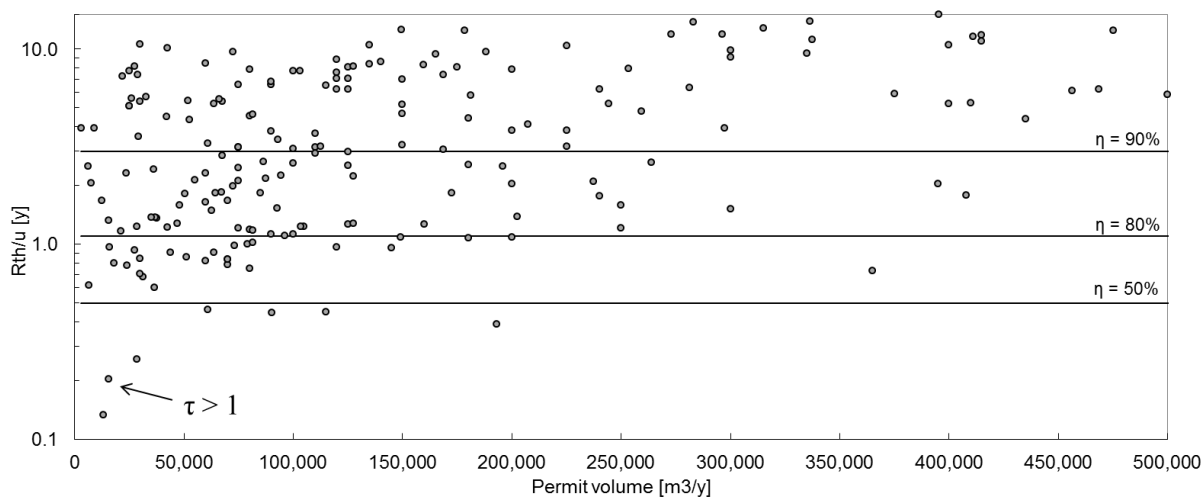
$$369 \quad A_{overlap} = \eta_{th} A_{footprint} \rightarrow A_{overlap} = \eta_{th} \pi R_{th}^2 \quad (11)$$

370 results in a relation between efficiency, flow velocity and the thermal radius;

$$371 \quad \eta_{th} = \frac{2}{\pi} a \cos\left(\frac{t_{sp}u_*}{2R_{th}}\right) - \frac{t_{sp}u_*}{\pi R_{th}^2} \sqrt{R_{th}^2 - \frac{1}{4}(t_{sp}u_*)^2} \quad (12).$$

372 For every ATES system with $\tau < 1$ the efficiency can be obtained with this relation. When $R_{th} > u$, the $t_{sp}u_*$ -term
 373 under the square root contributes less than 1% to the obtained efficiency. Under these conditions, both right and
 374 left term of Equation (12) depend on the ratio between the traveled distance and the thermal radius. So for any
 375 constant combination of u_* over R_{th} , the efficiency is the same, which allows to identify the efficiency as a
 376 function of the R_{th}/u -ratio for different storage periods, Figure 10 (bottom). This can be used to identify
 377 minimum desired thermal radius (i.e. maximum desired screen length for a given storage volume) at a location
 378 with a given groundwater flow velocity to meet a minimal efficiency.

379 The derived relation is now used to assess the well design data with respect to the local ambient groundwater
 380 flow velocity, hydraulic conductivity and thickness of the aquifer. For each of the ATEs systems in the dataset
 381 the R_{th}/u -value was determined, the relation given in Figure 10 (bottom) is used to indicate lines of expected
 382 thermal efficiency only taking into account losses due to displacement caused by ambient groundwater flow,
 383 Figure 11.



384

385 *Figure 11, R_{th}/u -values for ATEs systems in the dataset with thresholds for different thermal recovery efficiencies*

386 Figure 11 shows that about 20% of the systems have an expected efficiency lower than 80% ($R_{th}/u < 1.1$). For the
 387 ATEs systems with an expected efficiency lower than 80% (Table 4) the average storage volume is relatively
 388 small and the average flow velocity relatively high at 36 m/y. Although minimizing screen length reduces heat
 389 losses due to displacement, minimizing for conduction and dispersion losses require an optimal screen length for
 390 a particular storage volume.

391 *Table 4, Results of analysis of screen length with respect to groundwater flow velocity*

	average u	average V	average R_{th}
	[m/y]	[m ³ /y]	[m]
$\eta > 80 \%$	6	263,000	46
$\eta < 80 \%$	33	100,000	32

392 *Conclusion analytical analysis*

393 In optimizing the storage geometry of ATEs systems the applied length should be carefully considered.
 394 However, in both Figure 6 and Figure 9 it can be seen that many ATEs systems with varying storage volumes
 395 have identical screen lengths, at various multiplications of 5m. This likely relates to the fact that screen sections
 396 are supplied in 5 m sections, which can, but are not adjusted to a specifically required length. The wide range of
 397 storage volume per single screen length (e.g. 40,000 – 420,000 m³ for $L=20$, Figure 9) thus indicates that the

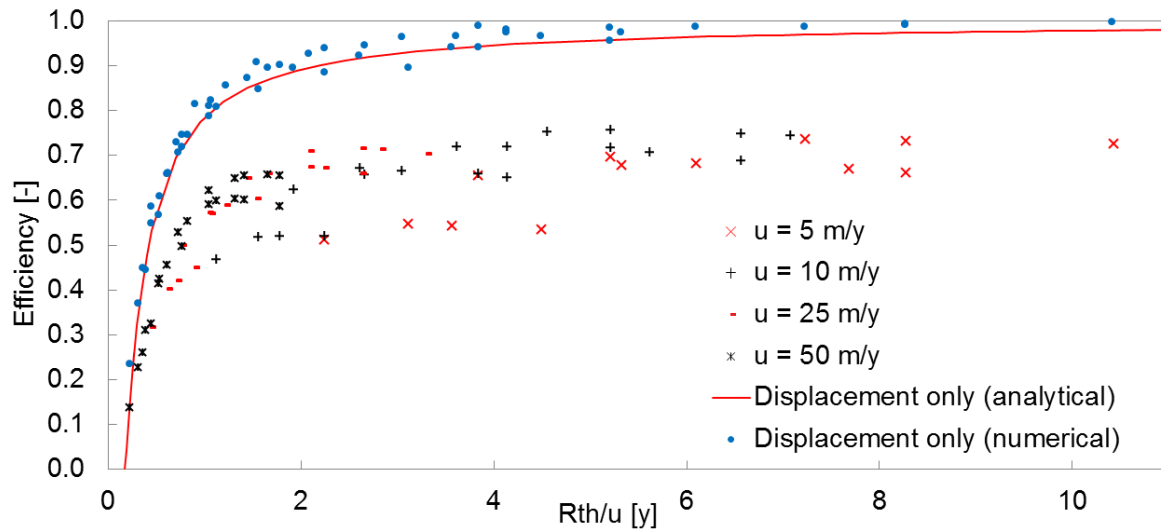
398 screen length design indicated in the permit application are generally not based on an evaluation of storage
399 volume and local geohydrological conditions, Dutch design standards only consider the clogging potential for
400 ATES well design (NVOE, 2006). Particularly for smaller ATES systems, the sensitivity of recovery efficiency
401 for screen length selection is high, as these are most vulnerable for significant losses as a consequence of
402 ambient groundwater flow and dispersion and conduction (Figure 8 and Figure 10).

403 **3.3 Numerical evaluation of energy losses**

404 To assess the combined effect of conduction, dispersion and displacement losses, the results of the performed
405 numerical MODFLOW simulations are discussed and compared with the straightforward and simple analytical
406 solutions presented in the previous section. The wide range of ATES conditions for which the numerical
407 simulations were performed resulted in recovery efficiencies between 10 and 70%.(Figure 12).

408 *Contribution of displacement losses*

409 The lowest efficiencies are associated with the scenarios with high ambient groundwater flow (>50 m/year),
410 together with relatively small thermal radius, which results in a small thermal radius over ambient groundwater
411 flow (R_{th}/u -ratio <1 y). For both the numerical and the analytical solution for the impact of ambient groundwater
412 flow on recovery efficiency is very sensitive for low R_{th}/u -values. However, at higher R_{th}/u -values (>1 y) the
413 efficiency becomes less dependent of R_{th}/u , as dispersion and conduction losses are dominant under such
414 conditions. In all cases the analytical solution overestimates the efficiency compared to numerical results,
415 because the analytical solution does not take account for conduction and dispersion losses. To estimate the
416 efficiency for the numerical simulations that would result under the impact of displacement only, the obtained
417 efficiencies under no flow conditions are used as a reference (following (D_u) for $u= 5$ m/y; $D_5=(1-\eta_0) + \eta_5$).
418 These numerically derived estimates show a good resemblance with the analytical relation. This confirms that
419 the analytical approach is valid to determine displacement losses separately.



420

421 *Figure 12, Relation between efficiency and thermal radius over groundwater flow velocity (R_{th}/u) for numerical simulation results and*
 422 *analytical solution (Equation (12)) for 0.5y storage period.*

423 *Contribution of conduction and dispersion losses*

424 Simulated efficiencies for the scenarios without ambient groundwater flow were highest, up to 75%, and highly

425 correlated with the surface area over volume ratio A/V (Figure 13), in contrast with the simulations with the

426 highest ambient groundwater flow (50 m/y). Also the A/V ratios calculated for earlier simulation studies and

427 experiments without ambient groundwater flow (Caljé, 2010; Doughty et al., 1982; Lopik et al., 2016) strongly

428 correlate with the observed efficiencies in these studies. Like in this study, the results from Lopik et al. (2016)

429 and Doughty et al. (1982) consist of a series systematic changing boundary conditions which allows for

430 verification of the relations found in Figure 13. Results of both Lopik et al. (2016) and Doughty et al. (1982)

431 show a linear relation with similar slope between the surface area over volume ratio (A/V) and efficiency in the

432 absence of ambient groundwater flow. The excellent correlation efficiency with the A/V ratio for each study with

433 no ambient groundwater flow, indicates that under similar condition the efficiency of ATEs systems for a

434 particular aquifer system and operational mode can be interpolated based on A/V .

435 Although similar, the efficiencies at a particular A/V ratio deviate for these different modeling studies and are

436 likely to be caused by small differences in parameters and model set-up. E.g.; both Doughty et al. (1982) and

437 Lopik et al. (2016) used an axisymmetric model and a finer vertical spatial discretization compared to this study,

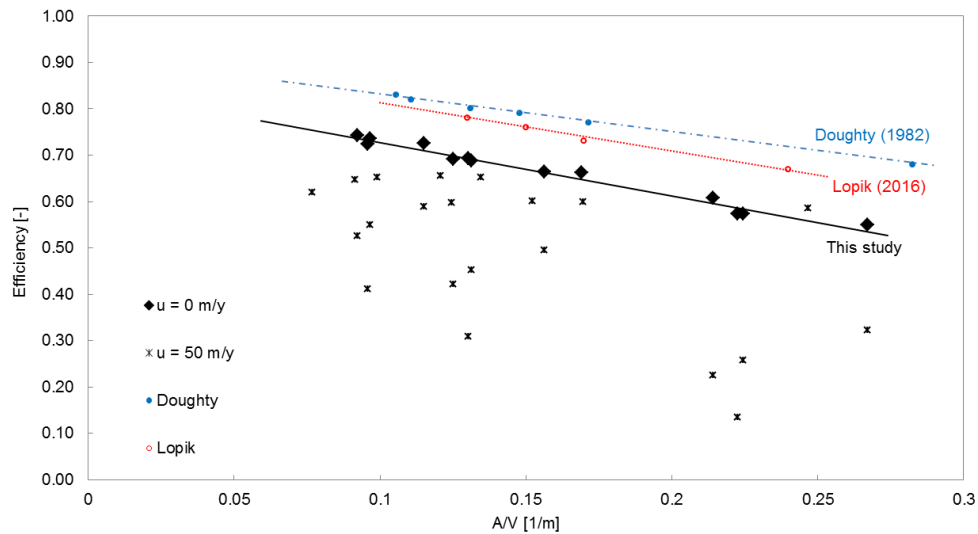
438 resulting in differences in numerical dispersion. Also, Doughty et al. (1982) uses no dispersion, which explains

439 why their simulations show the highest efficiency. Lopik et al. (2016) uses shorter and less storage cycles as

440 well as a slightly smaller dispersion coefficients compared to this study. From these (small) differences can be

441 seen that at simulations with higher dispersion, the A/V – efficiency relation becomes steeper, small systems

442 which have a larger A/V ratio then suffer relatively more, confirming the earlier observation from Figure 7 that
 443 at larger storage volumes conduction losses dominate.

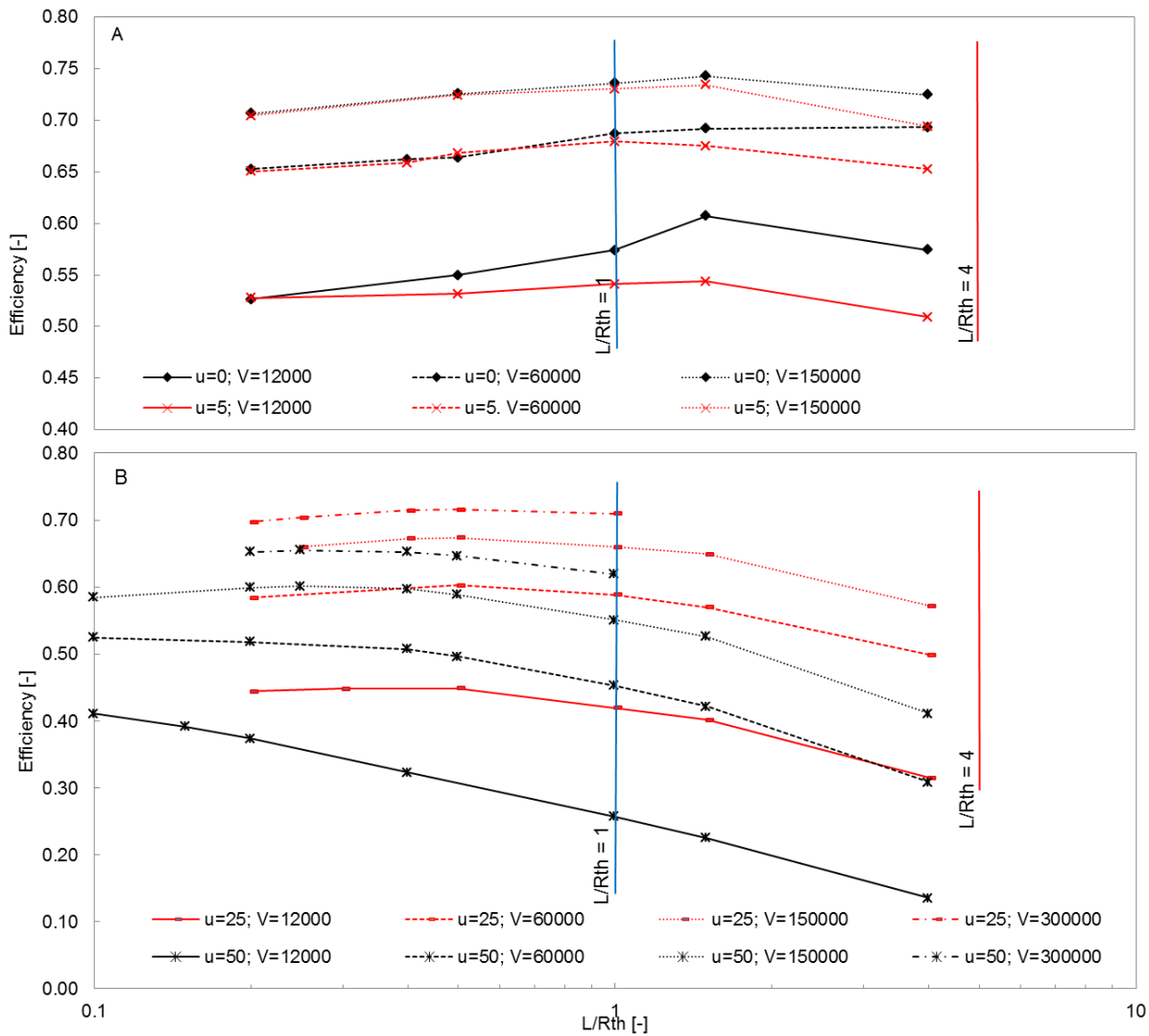


444

445 *Figure 13, Simulated efficiencies relative to geometric property (A/V) from this and other studies at u = 0 m/y and for u=50 m/y from the*
 446 *simulations done in this study. The Pearson correlation between A/V and efficiency is -0,99 for u = 0 m/y. and -0.58 for u= 50 m/y. From the*
 447 *Lopik et al (2016) study, only the data are used from the simulations that excluded buoyancy flow.*

448 *Combined displacement and conduction & dispersion losses*

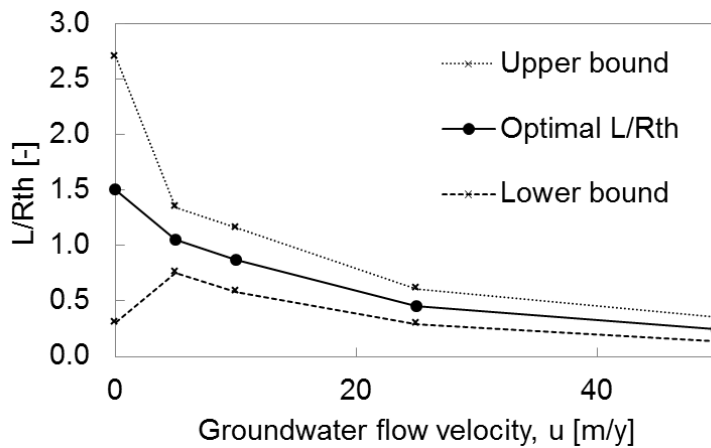
449 As found by Doughty et al. (1982) the optimum for L/R_{th} ratio for a particular ATEs storage volume is around
 450 1.5 in the absence of ambient groundwater flow. However this optimal ratio shifts to lower values with
 451 increasing ambient groundwater flow velocity (Figure 14). The optima remains flat for higher groundwater flow
 452 velocity, only for the smallest system (12,000 m³) at the highest ambient groundwater flow (50 m/y) tested, this
 453 is not the case within the simulated conditions.



454

455 *Figure 14. Simulated efficiencies for different groundwater flows (u) and screen length over thermal Radius (L/R_{th}) of various storage*
 456 *volumes. A. is at no/low ambient groundwater flow (Doughty applies). B. is at high ambient groundwater flow.*

457 To identify the optimal L/R_{th} at different rates of groundwater flow velocity, the L/R_{th} value of the simulation
 458 series of each storage volume and groundwater flow velocity with the highest efficiency was selected from the
 459 different L/R_{th} scenarios simulated. To take into account the flat optima also the L/R_{th} values with less than 5%
 460 deviation in efficiency were selected. For each of the simulated ambient groundwater flow velocity, the average
 461 and the standard deviation of the optimal L/R_{th} values were calculated and plotted in Figure 15. This empirical
 462 relation shows how the well design for ATEs wells can be optimized taking account conduction, dispersion and
 463 displacement losses. It also shows that at higher ambient groundwater flow, well design is more critical, since
 464 the allowed deviation of the optimal solution becomes smaller. Despite the limited number of simulations (120),
 465 the number and spreading of different conditions is sufficient to use this relation in design practice.



466

467 *Figure 15. Optimal L/R_{th} for different groundwater flows empirically derived from simulation results*

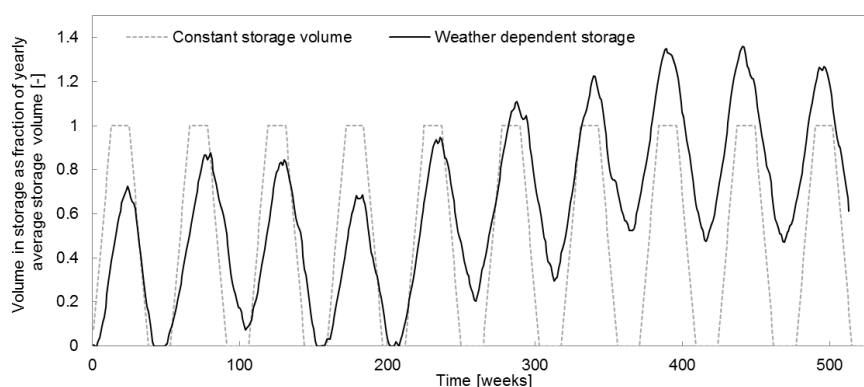
468 **4. Discussion**

469 *Size and variation in seasonal storage volume*

470 As shown in this research storage volume is an important parameter affecting recovery efficiency. In assessing
 471 this efficiency it has been assumed that the infiltrated and extracted volume is equal for each cycle. However, in
 472 practice the infiltration and extraction volume from wells are typically not equal due to variations in heating and
 473 cooling demand. This can have a significant influence on the perceived recovery efficiency per cycle.
 474 Monitoring data indicates energy imbalances varying between -22% and + 15% (Willemsen, 2016). Because in
 475 general ATEs systems have to meet energy balance for a certain period, in The Netherlands 3-5 years depending
 476 on provincial legislation, a representative storage volume can be used to assess conduction and displacement
 477 losses. Because the absolute losses increase with increasing storage volumes, it is more beneficial to optimize for
 478 maximum storage volume. This is also reflected in Equation (7) where can be seen that the A/V -value has a flat
 479 optimum at larger storage volumes (Figure 8), and also in the relation identified by Doughty et al. (1982) and
 480 shown in Figure 14. Therefore, the permitted capacity data of the ATEs wells in The Netherlands were used to
 481 compare theoretical well design approaches with field data, Figure 9. However, in practice ATEs systems
 482 deviate from their permit capacity to store heat because ATEs operators request a larger permit capacity to allow
 483 for flexibility during operation; e.g. building energy demand may be higher than expected, possible future
 484 growth, change of building function and seasonal fluctuations. This influences the shape and thus the losses of
 485 the heat storage. Operational data of ATEs systems from different databases have been used in regional and
 486 national studies and evaluations (CBS, 2005; Graaf et al., 2016; SIKB, 2015b; Willemsen, 2016) all showing that

487 ATES systems yearly actually only use 40-60 % of their initially requested and permitted capacity. The ranges of
488 systems sizes presented in this study, e.g. Figure 5 and Figure 6, are therefore much smaller in practice.

489 Also variations in seasons affect the total storage volume in the ATEs wells. In this study the common
490 assumption was made, that the average yearly volume is infiltrated and extracted during the winter and summer,
491 with a storage period in between, resulting in a block-scheme like infiltration, storage and extraction pattern.
492 However, heating and cooling demand typically does not balance perfectly during a year and seasonal variations
493 may cause temporal imbalances, resulting in a sometimes smaller and sometimes larger heat storage compared to
494 the yearly average storage. For example, heat may remain in warm wells during a couple of warm winters until a
495 colder winter depletes the warm well. The effect of this aspect is illustrated by the presentation of the cumulative
496 volume stored in a well relative to the average value for multiple years, Figure 16. This pattern is derived from
497 the storage volume variation based on the monitored and projected outside air temperature (2010-2020) of the
498 weather station of De Bilt in The Netherlands (KNMI, 2013). The energy demand pattern is determined by
499 deriving the energy demand for each day by scaling the yearly average energy demand to the deviation of the
500 daily temperature from the average outside air temperature of the evaluation period. As a result of this seasonal
501 variations imbalances occur over the years, resulting in varying stored volume in the wells. From Figure 16 can
502 be seen that the maximum storage capacity occurring in practice is around 150 % of the average yearly storage
503 volume. This exercise was done for different climatic datasets (monitored as wells as projections), all giving the
504 same outcome, that the maximum storage in the well is about 150% of the average yearly storage.



505
506 *Figure 16, Volume in storage of warm well for different energy demand patterns*

507 The fact that well design can be best determined for maximum storage volume, then leads to the conclusion that
508 150 % of the expected yearly average storage volume, which in turn is about 75% of the permitted capacity
509 (50% of permitted capacity is used in practice) must be used as a basis for well design. Correcting the data of the

510 permitted volumes for these two aspects results in the ATEs systems plotted in Figure 9 and Figure 11 to
511 respectively move up- and downwards.

512 *Additional well design criteria in practice*

513 The well design criteria required to assess and optimize the thermal recovery efficiency were considered in this
514 study. However, in practice additional aspects such as capacity, prevention of well clogging, available aquifer
515 thickness, mutual interaction and drilling and installation costs all play a role in determining the well design. In
516 practice the determination of screen length is mainly based on the maximum desired pumping rate (NVOE,
517 2006). Together with minimizing drilling costs this is a driver for screen lengths that are too short to achieve
518 optimal thermal efficiency, which is clearly reflected in Figure 9. In the Netherlands, a clear guideline or method
519 available to take account for losses as a result of ambient groundwater flow in well design is currently lacking
520 (NVOE, 2006), which is reflected in Figure 11. The effect of a partially penetrating well on the distribution and
521 A/V -ratio of heat is both not discussed in this study and not taken into account in current practice. However,
522 given the identified significant effect of the A/V -ratio on efficiency, the efficiency of a partially penetrating well
523 may deviate significantly from a fully penetrating well with the same storage volume and screen length. For
524 partially penetrating wells the aquifer anisotropy is also an important parameter to consider.

525 In this study is shown that suboptimal well design may have a large influence on well efficiency, but can also be
526 limited relatively easily. As shown in Figure 8 and Figure 14, the dependency for both A/V and L/R_{th} with
527 efficiency has a flat optimum beyond some threshold, which then allows dealing with local aquifer thickness
528 conditions and uncertainties in storage volume now this threshold is known.

529 *The impact of ambient groundwater flow on the efficiency of ATEs systems*

530 High ambient groundwater flow affects the recovery efficiency of ATEs systems significantly. The missing
531 framework to assess stored heat losses due to groundwater flow is introduced in this paper. Also the orientation
532 of ATEs wells with respect to the ambient flow direction needs to be taken into account. Warm and cold wells
533 need to be oriented perpendicular to the flow direction. For individual systems this framework helps to improve
534 well efficiency, a drawback of the presented framework is, however, the resulting large thermal radii and
535 suboptimal use of aquifer thickness. In areas with many ATEs systems close together this may lead to scarcity of
536 subsurface space for ATEs. In such busy areas with high ambient groundwater flow, planning strategies should
537 work towards placement of same type of wells in the direction of the groundwater flow, where then only the
538 most upstream wells will suffer from losses due to groundwater flow, for which compensation arrangements may

539 be made. Multi doublet systems on the other hand may better use the strategy to place well of the same type in
540 the direction of the flow and infiltrate relatively more heat in the upstream and extract more from the
541 downstream well to compensate for the ambient groundwater flow losses, as was described by Groot (2013).

542 *The effect of aquifer conditions*

543 The shape of the stored heat was assumed to have a cylindrical shape in this evaluation of well design. However,
544 in a heterogeneous aquifer the storage volume does not have the shape of a 'perfect' cylinder, resulting in a
545 varying thermal radius over the depth of the screen. As a consequence of heterogeneity the A/V -ratio in practice
546 is higher compared to the expected value for a homogeneous aquifer. Although they both use a single ATES
547 configuration, Sommer (2013) and Caljé (2010) show that the net effect of heterogeneity on efficiency is limited
548 over multiple storage cycles and its influence is much smaller compared to the effect of A/V and ambient
549 groundwater flow on the efficiency. Only when gravel layers are present such heterogeneity may affect
550 efficiency significantly, and should therefore best be blinded (Caljé, 2010). Next to variations in hydraulic
551 conductivity, also variations in salinity may affect the shape of the storage volume due to buoyancy flow due to
552 density differences. Such aspects will affect the efficiency dependencies derived for the homogeneous and
553 isotropic conditions evaluated in this study. Also the efficiency dependency for application of ATES in more
554 challenging geohydrological environments will require further study.

555 *Combined wells and mutual interaction*

556 This study focusses on optimizing the recovery efficiency of a single ATES systems and individual wells, ATES
557 systems however cumulate in urban areas (Bloemendal et al., 2014; Hoekstra et al., 2015) and regularly share
558 subsurface space to store or extract heat. As a consequence, additional considerations need to be taken into
559 account, which might lead to deviations from the design consideration presented in this research. For example,
560 planning of subsurface space occurs based on the thermal footprint (Figure 3) of an ATES well projected at
561 surface level (Arcadis et al., 2011; Li, 2014), which then promotes the use of longer screens. From the flat
562 optima shown in Figure 14 it can be seen that the individual well efficiency may not have to suffer much from
563 such additional consideration. This will allow larger number of ATES systems to be accommodated in such areas
564 and with that the overall CO₂ emission reduce (Jaxa-Rozen et al., 2015). Also, large ATES systems often have
565 multiple warm and cold wells which are placed together and function as one single storage in the subsurface. The
566 length of the screens of such combined wells should therefore also be determined based on the fact that they
567 function as one storage volume in the subsurface, disregarding this aspect gives a suboptimal A/V and amplifies
568 the effect of having a larger footprint, in areas where this must be prevented. From this is concluded that

569 combining wells, also requires a well design for the individual wells based on storage capacity of both wells
570 together. However, in such busy aquifers best would be to promote the use of the full aquifer thickness for wells
571 and use a full 3D planning strategy.

572 **5. Conclusion**

573 In this study an evaluation of ATES characteristics from practice together with analytical and numerical
574 simulations were used to develop the missing framework for ATES well design to achieve optimal recovery
575 efficiency. This work includes the losses due to heat displacement with ambient groundwater flow. The results
576 show that two main processes control thermal recovery efficiencies of ATES systems. These are due to the
577 thermal energy losses that occur 1) across the boundaries of the stored volume by mainly conduction and
578 dispersion only at smaller storage volumes and 2) due to the displacement of stored volumes by ambient
579 groundwater flow.

580 For the latter process, an analytical expression was deduced that suitably describes thermal recovery efficiency
581 as a function of the ratio of the thermal radius over ambient groundwater flow velocity (R_{th}/u). For the conditions
582 tested, at $R_{th}/u < 1$ the displacement losses were dominant and thus would require minimization of the well
583 screen length or maximize the volume stored. Obviously, practical aspects, such as required minimum well
584 capacity or the availability of suitable aquifers, may prevent the use of optimal screen lengths as is illustrated for
585 a large part (15%) of the evaluated Dutch ATES systems that indicate an efficiency of less than 50%, due to
586 ambient groundwater flow (Figure 11).

587 With respect to the dispersion and conduction losses it was shown that conduction is dominating and for the
588 numerical simulation results of this and previous studies, thermal recovery efficiency linearly increases with
589 decreasing surface area over volume ratios of the stored volume (A/V) for a particular set of operational and
590 geohydrological conditions. With respect to the losses due to conduction and dispersion, the optimal screen
591 length has a flat optimum, which allows to also take account for other considerations in well design like
592 neighboring systems and partially penetrating effects.

593 For the optimization of thermal recovery efficiency with respect to both main processes, the optimal value for
594 the ratio of well screen length over thermal radius (L/R_{th}) decreases with increasing ambient groundwater flow
595 velocities as well as its sensitivity for efficiency. With the insights on the controls on thermal recovery efficiency
596 derived in this study, the assessment of suitable storage volumes, as well as the selection of suitable aquifer

597 sections and well screen lengths, can be supported to maximize the thermal recovery of future seasonal ATES
598 systems in sandy aquifers world-wide.

599 *Acknowledgements*

600 This research was supported by Climate-kic E-use (aq) and the URSES research program funded by the Dutch
601 organization for scientific research (NWO) and Shell, grant number 408-13-030. We thank two anonymous
602 reviewers for their valuable comments on the manuscript.

603 **References**

- 604 Anderson, M.P., 2005. Heat as a ground water tracer. *Ground water* 43, 951-968.
- 605 Arcadis, TTE, Bos, W., 2011. *Handreiking masterplannen bodemenergie*. SKB, Gouda.
- 606 Bear, J., 1979. *Hydraulics of groundwater*. Dover Publications inc., Mineola, New York.
- 607 Bear, J., Jacobs, M., 1965. On the movement of water bodies injected into aquifers. *Journal of Hydrology* 3, 37-57.
- 608 Bloemendal, M., Olsthoorn, T., Boons, F., 2014. How to achieve optimal and sustainable use of the subsurface for Aquifer Thermal Energy
609 Storage. *Energy Policy* 66, 104-114.
- 610 Bloemendal, M., Olsthoorn, T., van de Ven, F., 2015. Combining climatic and geo-hydrological preconditions as a method to determine
611 world potential for aquifer thermal energy storage. *Science of the Total Environment* 538 621-633.
- 612 Bonte, M., 2013. *Impacts of shallow geothermal energy on groundwater quality, geo sciences*. Vrije Universiteit Amsterdam, Amsterdam.
- 613 Bonte, M., Mesman, G., Kools, S., Meerkerk, M., Schriks, M., 2013a. *Effecten en risico's van gesloten bodemenergiesystemen*. KWR
614 Watercycle research institute, Nieuwegein.
- 615 Bonte, M., Van Breukelen, B.M., Stuyfzand, P.J., 2013b. Environmental impacts of aquifer thermal energy storage investigated by field and
616 laboratory experiments. *Journal of Water and Climate Change* 4, 77.
- 617 Caljé, R., 2010. *Future use of aquifer thermal energy storage inbelow the historic centre of Amsterdam*, Hydrology. Delft University of
618 Technology, Delft.
- 619 CBS, 2005. *Hernieuwbare energie in Nederland 2004*, in: CBS (Ed.). Central authority for statistics in NL, Den Haag.
- 620 CBS, 2016a. *Issued building permits 1990-2015* retrieved from statline database, in: CBS (Ed.). Central authority for statistics in NL, Den
621 Haag.
- 622 CBS, 2016b. *Voorraad woningen en niet-woningen; mutaties, gebruiksfunctie, regio*. CBS.nl.
- 623 Ceric, A., Haitjema, H., 2005. On using Simple Time-of-travel capture zone delineation methods. *groundwater* 43, 403-412.
- 624 Doughty, C., Hellstrom, G., Tsang, C.F., 1982. A dimensionless approach to the Thermal behaviour of an Aquifer Thermal Energy Storage
625 System. *Water Resources Research* 18, 571-587.
- 626 EIA, 2009. *Residential Energy consumption survey*, US Energy Information Administration.
- 627 EU, 2010. *Directive on the energy performance of buildings*, in: Union, O.J.o.t.E. (Ed.), 153;13-35. EU-Parliament, European Union,
628 Strasbourg.
- 629 Eugster, W.J., Sanner, B., 2007. *Technological status of shallow geothermal energy in Europe*, European geothermal congress, Unterhaching,
630 Germany.
- 631 Fry, V.A., 2009. *Lessons from London: regulation of open-loop ground source heat pumps in central London*. Geological society of London
632 42, 325-334.
- 633 Gelhar, L.W., Welty, C., Rehfeldt, K.R., 1992. *A critical Review of Data on Field-Scale Dispersion in Aquifers*. *Water Resources Research*,
634 1955-1974.
- 635 Graaf, A.d., Heijer, R., Postma, S., 2016. *Evaluatie Wijzigingsbesluit bodemenergiesystemen*. Buro 38 in commision of ministry of
636 Infrastructure and environment, Cothen.
- 637 Groot, J., 2013. *Optimizing energy storage and reproduction for Aquifer Thermal Energy Storage*, Geosciences. University of Utercht.
- 638 Haehnlein, S., Bayer, P., Blum, P., 2010. *International legal status of the use of shallow geothermal energy*. *Renewable and Sustainable
639 Energy Reviews* 14, 2611-2625.
- 640 Harbaugh, A.W., Banta, E.R., Hill, M.C., McDonald, M.G., 2000. *Modflow-2000, the u.S. Geological survey modular ground-water
641 model—user guide to modularization concepts and the ground-water flow process* in: USGS (Ed.). US Geological Survey, Virginia.
- 642 Hartog, N., Drijver, B., Dinkla, I., Bonte, M., 2013. *Field assessment of the impacts of Aquifer Thermal Energy Storage (ATES) systems on
643 chemical and microbial groundwater composition*, European Geothermal Conference, Pisa.

644 Hecht-Mendez, J., Molina-Giraldo, N., Blum, P., Bayer, P., 2010. Evaluating MT3DMS for Heat Transport Simulation of Closed
645 Geothermal Systems. *Ground water* 48, 741-756.

646 Hoekstra, N., Slenders, H., van de Mark, B., Smit, M., Bloemendal, M., Van de Ven, F., Andreu, A., Sani, D., Simmons, N., 2015. Europe-
647 wide Use of Sustainable Energy from Aquifers, Complete report. Climate-KIC.

648 Jaxa-Rozen, M., Kwakkel, J.H., Bloemendal, M., 2015. The Adoption and Diffusion of Common-Pool Resource-Dependent Technologies:
649 The Case of Aquifer Thermal Energy Storage Systems, PICMET, Portland.

650 Kasenow, M., 2002. Determination of Hydraulic Conductivity from grain size Analysis. Water Resources publications LLC, Highlands Ranch
651 Colorado.

652 Kim, J., Lee, Y., Yoon, W.S., Jeon, J.S., Koo, M.-H., Keehm, Y., 2010. Numerical modeling of aquifer thermal energy storage system.
653 *Energy* 35, 4955-4965.

654 KNMI, 2013. Hourly data 1980-2010, climatic projections KNMI W+ scenario 2010-2045 for Weather station 260, de Bilt.

655 LGR, 2012. Dutch register/database for groundwater abstractions, in: Netherlands, P.o.T. (Ed.).

656 Li, Q., 2014. Optimal use of the subsurface for ATEs systems in busy areas, Hydrology. Delft University of Technology, 2014.

657 Lopik, J.H.v., Hartog, N., Zaadnoordijk, W.J., 2016. The use of salinity contrast for density difference compensation to improve the thermal
658 recovery efficiency in high-temperature aquifer thermal energy storage systems. *Hydrogeology Journal*.

659 Ministry-of-Internal-affairs, 2012. Bouwbesluit (Building Act). Ministry-of-Internal-affairs, Den Haag.

660 Molz, F.J., Melville, J.G., Parr, D.D., King, D.A., Hopf, M.T., 1983. Aquifer Thermal Energy Storage' A Well Doublet Experiment at
661 Increased Temperatures. *Ground water* 19, 149-160.

662 Molz, F.J., Warman, J.C., Jones, T.E., 1978. Aquifer Storage of heated water. *Groundwater* 16.

663 Nagano, K., Mochida, T., Ochifuji, K., 2002. Influence of natural convection on forced horizontal flow in saturated porous media for aquifer
664 thermal energy storage. *Applied Thermal Engineering* 22 1299–1311.

665 NVOE, 2006. Richtlijnen Ondergrondse Energieopslag, Design guidelines of Dutch branche association for geothermal energy storage,
666 Woerden.

667 Réveillère, A., Hamm, V., Lesueur, H., Cordier, E., Goblet, P., 2013. Geothermal contribution to the energy mix of a heating network when
668 using Aquifer Thermal Energy Storage: Modeling and application to the Paris basin. *Geothermics* 47, 69-79.

669 RHC, 2013. Strategic Research and Innovation Agenda for Renewable Heating & Cooling. Renewable Heating & Cooling, European
670 Technology Platform, Brussels.

671 SER, 2013. Energie Akkoord. Social economical council.

672 SIKB, 2015a. BRL 2100 Mechnisch boren. SIKB, Gouda.

673 SIKB, 2015b. Userdata of ATEs systems, in: NL, d.p.i. (Ed.). recieved from 4 provinces of the Netherlands in 2015, Gouda.

674 Sommer, W., 2015. Modelling and monitoring Aquifer Thermal Energy Storage. Wageningen University, Wageningen.

675 Sommer, W., Valstar, J., van Gaans, P., Grotenhuis, T., Rijnaarts, H., 2013. The impact of aquifer heterogeneity on the performance of
676 aquifer thermal energy storage. *Water Resources Research* 49, 8128-8138.

677 Sommer, W.T., Doornenbal, P.J., Drijver, B.C., van Gaans, P.F.M., Leusbrock, I., Grotenhuis, J.T.C., Rijnaarts, H.H.M., 2014. Thermal
678 performance and heat transport in aquifer thermal energy storage. *Hydrogeology Journal* 22, 263-279.

679 TNO, 2002a. Boringen uit Dinoloket, digitale grondwaterkaart, Utrecht.

680 TNO, 2002b. REGIS, Utrecht.

681 Tsang, C.F., 1978. Aquifer thermal energy storage, in: Institute of Gas Technology Symposium on Advanced Technologies for Storing
682 Energy, C., IL, J.-., 1978 (Eds.).

683 UN, 2015. Adoption of the paris agreement. United Nations, Framework Convention on Climate Change, Paris.

684 Visser, P.W., Kooi, H., Stuyfzand, P.J., 2015. The thermal impact of aquifer thermal energy storage (ATES) systems: a case study in the
685 Netherlands, combining monitoring and modeling. *Hydrogeology Journal* 23, 507-532.

686 Willemsen, N., 2016. Rapportage bodemenergiesystemen in Nederland. RVO / IF technology, Arnhem.

687 Zeghici, R.M., Oude Essink, G.H.P., Hartog, N., Sommer, W., 2015. Integrated assessment of variable density–viscosity groundwater flow
688 for a high temperature mono-well aquifer thermal energy storage (HT-ATES) system in a geothermal reservoir. *Geothermics* 55, 58-68.

689 Zheng, C., Wang, P.P., 1999. MT3DMS: A Modular Three-Dimensional Multispecies Transport Model for Simulation of Advection,
690 Dispersion, and Chemical Reactions of Contaminants in Groundwater Systems; Documentation and User's Guide.

691 Zuurbier, K.G., Hartog, N., Valstar, J., Post, V.E., van Breukelen, B.M., 2013. The impact of low-temperature seasonal aquifer thermal
692 energy storage (SATES) systems on chlorinated solvent contaminated groundwater: modeling of spreading and degradation. *Journal of*
693 *contaminant hydrology* 147, 1-13.

694